Ellis, R. R. Inners, *J. Phys. Chem.* **86**, 867 (1982).
29. C. S. Yannoni, V. Macho, P. C. Myhre, *J. Am. Chem. Soc.* **104**, 907 (1982); *ibid.*, p. 7380; N. M. Szeverenyi, A. Bax, G. E. Maciel, *ibid.* **105**, 2579 (1983).
30. M. M. Maricq and J. S. Waugh, *Chem. Phys. Lett.* **47**, 327 (1977); *J. Chem. Phys.* **70**, 3300 (1979).
31. W. T. Dixon, *J. Magn. Reson.* **44**, 220 (1981); ———, J. Schaefer, M. D. Sefcik, E. O. Stejskal, R. A. McKay, *ibid.* **45**, 173 (1981); W. T. Dixon, J. Schaefer, M. D. Sefcik, E. O. Stejskal, R. A. McKay, *ibid.* **49**, 341 (1982); W. T. Dixon, *J. Chem. Phys.* **77**, 1800 (1982).
32. W. P. Aue, D. J. Ruben, R. G. Griffin, *J. Chem. Phys.* **80**, 1729 (1984).
33. S. J. Opella and M. H. Frey, *J. Am. Chem. Soc.* **101**, 5854 (1979); L. B. Alemany, D. M. Grant, T. G. Alger, R. J. Pugmire, *ibid.* **105**, 6697 (1983).
34. P. Caravatti, G. Bodenhausen, R. R. Ernst, *Chem. Phys. Lett.* **89**, 363 (1983); J. E. Roberts, S. Vega, R. G. Griffin, *J. Am. Chem. Soc.* **106**, 2506 (1984).
35. K. W. Zilm and D. M. Grant, *J. Magn. Reson.* **48**, 524 (1982); T. Terao, H. Miura, A. Saika, *J. Chem. Phys.* **75**, 1573 (1981).
36. L. Mayne, R. J. Pugmire, D. M. Grant, *J. Magn. Reson.* **56**, 151 (1984); T. Terao, H. Miura, A. Saika, *J. Am. Chem. Soc.* **104**, 529 (1982).
37. T. H. Maugh II, *Science* **224**, 793 (1984); D. P. Weitekamp, A. Bielecki, K. Zilm, A. Pines, *Phys. Rev. Lett.* **50**, 1807 (1983); A. Bielecki *et al.*, *J. Chem. Phys.* **80**, 2232 (1984).
38. A. Bax, *Two-Dimensional Nuclear Magnetic Resonance in Liquids* (Reidel, Boston, 1982).
39. A. Bax, N. M. Szeverenyi, G. E. Maciel, *J. Magn. Reson.* **52**, 147 (1983); N. M. Szeverenyi, A. Bax, G. E. Maciel, *ibid.*, in press.
40. A. Bax, N. M. Szeverenyi, G. E. Maciel, *ibid.* **55**, 494 (1983).
41. N. M. Szeverenyi and G. E. Maciel, *ibid.*, in press.

Nuclear Magnetic Resonance Technology for Medical Studies

Thomas F. Budinger and Paul C. Lauterbur

Nuclear magnetic resonance (NMR) applications to medical science began nearly 30 years ago with proton NMR measurements on cells, excised frog muscles, arms of living humans, and the living rat (*1*). Based on the observations in 1971 that the proton NMR properties of normal and malignant rat tissues differ (*2*) and in 1972 that NMR can be used to form images (*3*), technological and commercial activities of increasing intensity have focused on proton NMR imaging of the human body. At present, NMR imaging provides an anatomical description of soft tissues with a better contrast resolution than x-ray computed tomography (CT) in most areas of the body. Following the discovery of the relation between the phosphorus NMR spectra and the metabolites of red blood cells, in vivo evaluations of the concentration of high-energy phosphate compounds such as adenosine triphosphate (ATP) and creatine phosphate as well as cellular *p*H have found clinical applications (*4*). More recently, use of ^{1}H and ^{13}C spectra to evaluate other compounds has shown equally important potentials for clinical studies (*5*).

Summary. Nuclear magnetic resonance proton imaging provides anatomical definition of normal and abnormal tissues with a contrast and detection sensitivity superior to those of x-ray computed tomography in the human head and pelvis and parts of the cardiovascular and musculoskeletal systems. Recent improvements in technology should lead to advances in diagnostic imaging of the breast and regions of the abdomen. Selected-region nuclear magnetic resonance spectroscopy of protons, carbon-13, and phosphorus-31 has developed into a basic science tool for in vivo studies on man and a unique tool for clinical diagnoses of metabolic disorders. At present, nuclear magnetic resonance is considered safe if access to the magnet environment is controlled. Technological advances employing field strengths over 2 teslas will require biophysical studies of heating and static field effects.

This article is a report on the status of nuclear magnetic resonance imaging from theoretical and clinical viewpoints as expressed at a National Academy of Sciences symposium held in late 1983 (*6*), with a review of additional relevant information on in vivo spectroscopy reported in the literature through early 1984. A description of NMR theory and relaxation parameters relevant to NMR imaging is followed by an analysis of modern imaging strategies, signal-to-noise ratio, contrast agents, in vivo spectroscopy, spectroscopic imaging, clinical applications, and safety.

The theory of NMR is reviewed in a number of recent sources (*7*). Most elements have at least one reasonably abundant isotope whose nucleus is magnetic. The magnetic nuclei or nuclear spins of high abundance in biological material are ^{1}H, ^{13}C, ^{23}Na, ^{31}P, and ^{39}K. In an external magnetic field these nuclear spins behave like small magnets and assume a low-energy state aligned with the field or a higher energy state aligned against the field. The hydrogen nucleus (proton) is abundant in the body because of the high water content of nonbony tissues. When the body is immersed in a static magnetic field, slightly more protons become aligned with the magnetic field than against the static field. At 0.25 T (2500 gauss) and 25°C the difference between these aligned populations of about one proton in a million produces a net magnetization. A rapidly alternating magnetic field at an appropriate radio frequency (RF), applied by a coil near the subject or specimen in the static magnetic field, changes the orientation of the nuclear spins relative to the direction of the strong static magnetic field (Fig. 1). The changes are accompanied by absorption of energy by protons which undergo the transition from a lower energy state to the higher energy state. When the alternating field is turned off, the nuclei return to the equilibrium state with the emission of energy at the same frequency as that of the stimulating alternating field (RF). That frequency is the resonance or Larmor frequency, given by $\nu = (\gamma/2\pi)B$, where γ is the characteristic gyromagnetic ratio of the nucleus and B is the static magnetic field. The nuclei of different elements, and even of different isotopes of the same element, have very different resonance frequencies.

Thomas F. Budinger is Henry Miller Professor at Donner Laboratory, Lawrence Berkeley Laboratory, and the Department of Electrical Engineering and Computer Sciences, University of California, Berkeley 94720, and the Department of Radiology, University of California, San Francisco 94122. Paul C. Lauterbur is University Professor, Professor of Chemistry, and Research Professor of Radiology, Department of Chemistry, State University of New York, Stony Brook 11794.

For a field of 0.1 T (1000 gauss) the resonance frequency of protons is 4.2 MHz and that of phosphorus is 1.7 MHz. Thus, the magnetic nuclei in the body, when placed in a static magnetic field, can be made to act as receivers and transmitters of RF energy.

Relaxation Parameters

The physical-chemical properties of the tissue and the molecular environment of the nuclei are reflected in the time variation in the amplitude of the RF signal. This variation is a consequence of the interaction of the nuclear spins with a fluctuating magnetic field produced by nearby magnetic moments, including other similar and dissimilar nuclei as well as paramagnetic ions. The imposed RF energy is designed to perturb the thermal equilibrium of the magnetized nuclear spins, and the time dependence of the received signal is determined by the manner in which this system of spins returns to its equilibrium magnetization. The return is characterized by two parameters: T_1, the longitudinal relaxation time, describes the behavior of the component of the magnetization vector parallel to the applied static field B_0; and T_2, the transverse relaxation time, describes the behavior of the component of the magnetization vector transverse to B_0. Each component "relaxes" to its equilibrium value; the first is precisely the equilibrium magnetization, which is along B_0, and the second is zero at equilibrium. One can think of T_2 as a time for the nuclear spins to lose coherence (dephase).

The T_2 and T_1 values of pure water are about 2 seconds at 25°C and are nearly independent of B_0 for the field strengths considered here. Addition of solutes such as proteins shortens these times considerably to an extent that is a function of B_0. This has been investigated extensively for solutions of diamagnetic proteins (*8*) and for proteins containing paramagnetic ions (*9*). The results and insights gained by studying solutions of known composition can be readily transferred to investigations of the relaxation times of tissue, including the effects of paramagnetic ions (*10*).

To the extent that T_1 and T_2 are tissue-specific, these differences can be exploited to delineate different tissues in NMR images. The reasons for the differences in relaxation behavior of different tissues are not yet known, but it is known that the variation in water content, though it can affect relaxation, is not sufficient to explain all the differences observed (*11*).

Table 1. Typical NMR signal intensities in T_2-weighted imaging, decreasing top to bottom.*

Fat
Marrow and cancellous bone
Brain and spinal cord
Liver, spleen, pancreas
Muscle, kidney
Ligaments and tendons
Blood vessels with rapid flow
Compact bone
Air

*Pulse sequence and state of hydration can change ranking.

Among the fundamental factors influencing the differences will be the distribution of protein size in any tissue as well as the presence of fixed surfaces and interfaces (membranes, cytoskeletons, and so on) with which tissue water can interact (*12*).

Relaxation times can be measured at each point of an image (*13*). Because differences in tissue relaxation times determine image contrast, data on the relaxation behavior of different tissues as a function of static field strength B_0 are important in the selection of the optimal field strength and RF pulse sequence (for instance, spin-echo or inversion recovery) for acquisition of NMR images.

For spin-echo imaging, a commonly used imaging technique, the signal amplitude is given by (*14*)

$$S \simeq N f(v) (e^{-TE/T_2}) (1 - e^{-TR/T_1}) \quad (1)$$

where N is the concentration of nuclei (local spin density), $f(v)$ is the signal modulation due to moving nuclei (blood flow), TE is the elapsed time between the 90° RF pulse and the reception of a spin-echo signal; and TR is the repetition rate between successive spin-echo sequences (*15*). A decrease in T_1 or an increase in T_2 results in an increase in the NMR signal. Fat has a shorter T_1 and longer T_2 than other soft tissues; thus the NMR signals from fat produce the strongest signals in proton imaging.

Signal intensities from normal tissues will change significantly as the TE and TR timing parameters of the spin-echo sequences are changed, but in general the ranking of intensities of signals from normal tissues is that shown in Table 1. Tumors and abscesses with T_1's and T_2's longer than those of the normal tissues can be demonstrated with good contrast by choosing a pulse sequence which takes the best advantages of the differences between the relaxation parameters of the diseased tissue and those of the normal tissue. The relations between T_1 and T_2 and imaging contrast are shown in Fig. 2 for both the single spin-echo pulse sequences and the inversion recovery sequence (*15*), which is frequently used when differences in T_1 are being imaged. For inversion recovery, high contrast is accomplished by first inverting the magnetization with a 180° pulse and then allowing the magnetization to recover toward equilibrium for a time interval (TI) before applying a 90° RF pulse. Only the absolute value of the signal, which is positive whether the magnetization is along or against B_0, is usually detected. The contrast differences will depend on the T_1 differences and the TI chosen for imaging. Multiple-echo pulse sequences are also used, with late echoes used to observe signals with long T_2 at high contrast after those with shorter T_2 values have decayed.

The ability to accurately quantify relaxation rates in vivo is important for understanding and optimizing image contrast. Pure T_1 and pure T_2 images can be computed from data acquired with more than one RF pulse sequence (*14*); and

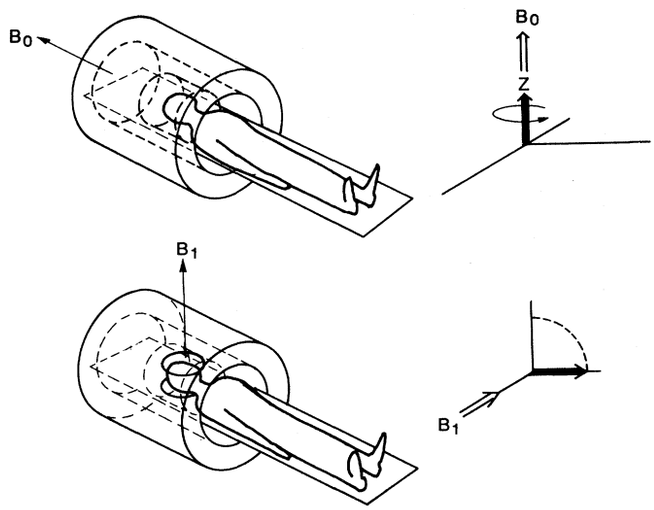

Fig. 1. Schematic of the NMR method. A static field B_0 is used to align spinning nuclei with magnetic moments. A relatively weak RF magnetic field B_1, generated from the RF coils surrounding the patient, perturbs the aligned nuclei. A voltage is generated by the interaction of the magnetic field from these nuclei with the coil. The strength and time dependence of this voltage convey information about the concentration and chemical environment of the nuclei.

these representations can be combined to reconstitute computed images which retrospectively optimize contrast between normal and abnormal tissues. Unfortunately, measurements of T_1 and T_2 are subject to large errors from blood flow artifacts, patient motion, RF field inhomogeneity, RF pulse sequence effects, and the multiexponential relaxation behavior of many tissues (*11*). Furthermore, selective excitations result in a variation of the tip angles through a slice. Thus, the conditions for accurate measurements of relaxation times will not in general be satisfied throughout the volume of the slice. In addition, diffusion will result in an erroneously low value of T_2 if selective excitations are used (*16*). As a result, the apparent relaxation times will be technique-dependent in ways which have not yet been fully analyzed. Full three-dimensional volume imaging methods involve simultaneous excitation of the whole volume; thus these techniques appear optimum from the standpoints of relaxation measurements and insensitivity to flow and motion.

Imaging Strategies

The frequency of the NMR signal is proportional to the magnetic field strength. Thus, if the field is varied across an object, the signal frequency will depend on the position of the transmitting nuclei in the object. The strength of the signal at each frequency can be interpreted as the nuclear magnetization in a plane within the object where the magnetic field corresponds to that frequency (*3*).

In order to obtain spatial information, some early systems employed a-c magnetic gradients to define "sensitive lines" or "sensitive points," which were translated electronically (*17, 18*), or mechanically, through the image space to obtain the corresponding information (*19*). These early methods have been supplanted by other methods made practical by recent advances in digital electronics and computer hardware.

Combinations of gradients in different directions can be used to select points, lines, or planes within the body. Selection of planes or "slices" is most commonly used in imaging strategies. These can be oriented in any direction, in contrast to the usual transaxial slice orientation of x-ray CT. By application of a gradient during the application of a narrow RF band, the protons are excited in a plane whose position and thickness depend on the RF pulse shape (*19*).

Once the plane has been selected, for example, by a z gradient, then x and y gradients are employed to determine the location within the selected x-y plane of the spin density and relaxation parameters. In the well-known projection method the NMR signal is encoded by using magnetic field gradients applied in different directions, so that the NMR spectrum corresponds directly to spatial projections (*4, 20*). If broadband pulses are used to excite the system in the presence of a linear gradient, the Fourier transform of the received signal is equal to the projection of the signals from all nuclei within the planes perpendicular to the line. The projection slice theorem is used to create two- and three-dimensional images, using algorithms somewhat similar to those used for x-ray CT (*20*). Since all of the nuclei in the tissue volume (or plane, in the two-dimensional case) being imaged are excited during each pulse, this technique is capable of achieving the highest signal-to-noise ratio possible for a given resolution per unit acquisition time (*21*). Because time must be allowed for the spins to relax after each pulse, there are limits to the minimum performance time required to produce an image.

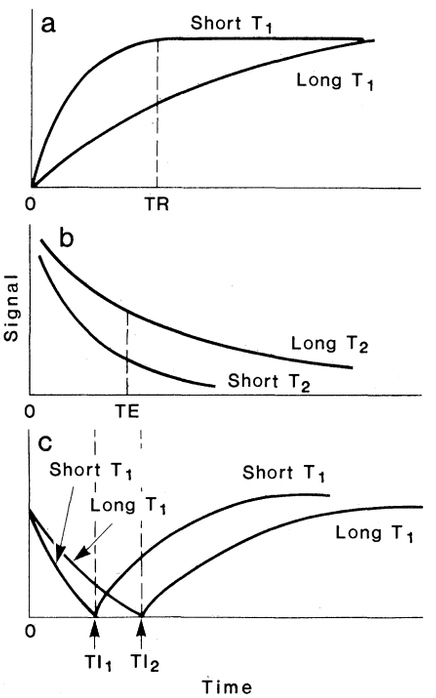

Fig. 2. The NMR proton image contrast between normal and pathological tissue depends on differences in T_1 and T_2 relaxation times and, to a lesser extent, on differences in spin density. Optimal contrast is dependent on the particular pulse sequence timing. (a) For spin-echo imaging (*15*), the interval between pulses TR will dictate the contrast between tissues with different T_1's. (b) Spin-echo timing TE will control the contrast between tissues with different T_2's. (c) Inversion recovery sequences (*15*) are useful for demonstration of T_1 differences. The direction of the difference depends on the difference in T_1's as well as on the time interval TI between the 180° and 90° RF pulses [for example, changing the interval between TI_1 and TI_2 would reverse the contrast for tissues with the T_1's shown in (c)].

Another class of methods—two-dimensional Fourier transform (*22*), spin-warp (*23*), echo planar (*18, 24*)—use gradients of varying magnitude to phase-encode the detected signals and thereby provide spatial information after multiple Fourier transformation of the encoded signals. The signal-to-noise ratio per unit acquisition time and the performance time are close to those of projection imaging. Extensions of this method for spectroscopic imaging are straightforward, though the computational and data acquisition problems are large. There are also engineering difficulties associated with coupling between the rapidly pulsed gradient coils and the rest of the system.

Echo planar imaging (*24*) offers faster image acquisition than other techniques and has been used to produce images of the beating heart. This technique employs multiple spin echoes produced in oscillating gradients during the single transient signal known as the free induction decay (FID) following one pulse.

Both categories are encoding procedures in which spatially and temporally varying magnetic fields are used to generate signals which can be referred to as reciprocal-space data. The decoding procedure involves an inversion process which is almost invariably accomplished by Fourier transformation.

A comprehensive conceptualization of the NMR imaging process has recently been used to describe and analyze both new and old imaging strategies (*25*). The method is known as the k-trajectory formulation. The time-varying gradients map the spatial-frequency domain of the object into the FID signal. The strategy or path of sampling the spatial-frequency domain is known as the k-trajectory (Fig. 3).

The observed signal in this type of NMR imaging experiment is composed of a time-varying signal which depends on T_2 and the fact that the observed RF phase at point $\mathbf{r}$ in the subject is $2\pi\gamma \int \mathbf{G}(t)dt$

$$\mathbf{S}(t) = \eta \int d\mathbf{r}\rho(\mathbf{r})\, e^{-t/T_2}\, e^{-2\pi i\mathbf{r}\gamma\int t\mathbf{G}(t')dt'} \quad (2)$$

where η represents the efficiency of the receiver coil detection circuit and is assumed to be 1.0, $\rho(\mathbf{r})$ the spin density, T_2 the transverse relaxation time, and $\mathbf{G}$ the field gradient. The Fourier transform of the spin densities is

$$\mathfrak{F}(\rho(\mathbf{k})) = \int d\mathbf{r}\ \rho(\mathbf{r})\, e^{-2\pi i\mathbf{r}\cdot\mathbf{k}(t)} \quad (3)$$

... neglect ... The off-resonance frequencies are neglected as well. Thus, from Eq. 2 we have

$$\mathbf{S}(t) = \mathfrak{F}\{\rho(\mathbf{k}(t))\} \tag{4}$$

with $\mathbf{k}(t)$ defined as the time integral of the gradient field

$$\mathbf{k}(t) = \gamma \int^t \mathbf{G}(t')\, dt' \tag{5}$$

Thus, the amplitude of the FID signal is

$$\mathbf{S}(t) = \int d\mathbf{r}\, \rho(\mathbf{r})\, e^{-i2\pi \mathbf{r}\cdot\mathbf{k}(t)} \tag{6}$$

Consequently, we now have a uniform method for describing and comparing different NMR imaging strategies. As an example, we note that in Fig. 3 simple projection imaging and the echo planar method (*24*) can be described with equal ease.

Another technique that uses RF field gradients instead of magnetic field gradients for encoding spatial information has been developed by Hoult (*26*). This method (rotating frame zeumatography) avoids difficulties associated with rapid switching of magnetic field gradients and is potentially useful for flow imaging and high-resolution chemical shift imaging.

Signal-to-Noise Ratio

An ongoing effort by all NMR imaging researchers and manufacturers is devoted to optimizing the signal-to-noise ratio. The NMR signal is proportional to the square of the NMR frequency ν and the noise is from the RF coil and the object in the coil. Thus, if the NMR spectrometer electronics are optimized and dielectric losses minimized (for example, by placing a Faraday screen between the coil and the patient), the signal-to-noise ratio for a spherical sample in a solenoidal coil is proportional to

$$\frac{\nu^2}{(\alpha a^2 \nu^{1/2} + \beta \nu^2 b^5)^{1/2}} \tag{7}$$

where a and b are the coil and sample radii, respectively, α and β are constants, and the two terms in the denominator represent contributions from coil and sample (*27*).

Signal losses in the patient cannot be reduced; improvements in the signal-to-noise ratio can be achieved only by increasing the magnetic field strength or reducing other sources of noise. The coil can be considered optimum when its noise contribution is much less than the body's contribution. A measure of this ratio is the change in quality factor Q when an unloaded coil is loaded with an object. For example, with an unconventional slotted tube resonator head coil (*28*), a Q value of 224 for the unloaded coil changed to a value of 25 when the coil was loaded with the head, indicating that the ohmic losses in the head were eight times those in the coil.

When the dominant noise source is the patient, the signal-to-noise ratio can be improved by minimizing the noise contribution from tissue other than that from which data are being collected. For this purpose surface coils and coils enclosing parts of the patient are used. Such coils often have very inhomogeneous RF fields, which result in uneven image brightness, but this can be compensated for as long as the signal-to-noise ratio is adequate throughout the region of interest. The goal in design is a configuration with high sensitivity in the region being imaged and low sensitivity elsewhere.

Increasing the field strength is probably the most direct means of improving the signal-to-noise ratio, assuming that the electronics and coil performance remain optimized. An 11-fold improvement in signal-to-noise ratio for a 63-MHz (1.5-T system) over a system operating at 5.1 MHz has been measured (*28*). This result is roughly in accord with Eq. 7. Other experiments with different assumptions about coil design indicate that the signal-to-noise advantage of increasing the B_0 field might be less than these predictions (*29*). There are three other aspects of the problem of determining the appropriate field strength. Relaxation times for protons usually increase with field, thus the time required to execute equivalent pulse sequences is longer. The increased strength of the magnetic fields in the environment of the magnet may also be a problem, as a field of 1 mT (10 gauss) can, for example, affect cathode-ray tube displays and pacemakers. It is likely that iron shielding will reduce the latter problem in the future. The increased potential for RF heating at the higher frequencies, along with decreased RF penetration, places an upper bound on the field strength useful for proton imaging.

Contrast Agents

The fact that relaxation behavior can be altered by use of pharmacological agents attached to paramagnetic ions such as those of manganese and gadolinium has led to an intense effort to use exogenously administered contrast agents with NMR. Paramagnetic ion agents (*30*) and nitroxide stable free radicals (NSFR's) (*31*) are two general classes of agents designed to modify tissue relaxation times. Paramagnetic ions and stable free radicals can facilitate energy exchange and dramatically decrease T_1 and T_2.

The local magnetic field of a paramag-

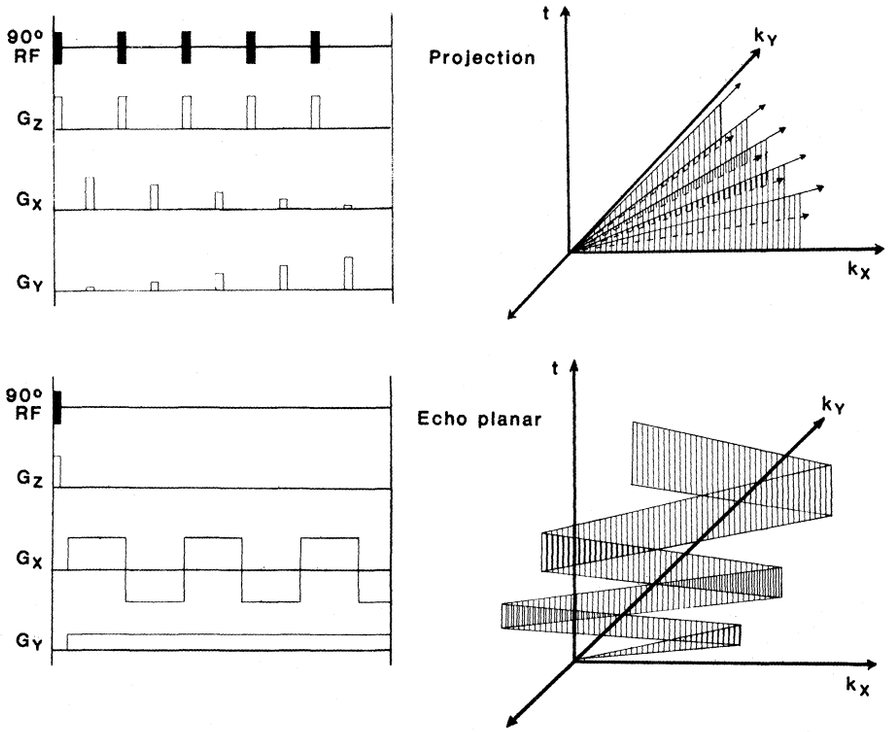

Fig. 3. Imaging strategies can be described by the temporal changes in RF and gradient pulses (left). The methods can also be envisioned as a k-trajectory map, which shows how reciprocal space is explored by changes in the x, y, and z magnetic field gradients during signal acquisition.

netic molecule will serve to increase the magnetic relaxation rates of surrounding hydrogen nuclei (*9, 32*). This relaxation effect is dependent on many variables, two of which are the concentration of the paramagnetic agent and the distance from the paramagnetic center to the hydrogen nucleus.

Data have been presented demonstrating the clinical potential of NSFR's (*31*). Nitroxide stable free radicals in millimolar concentrations have been shown to alter tissue relaxation times and appear to have potential use in evaluation of the blood-brain barrier (BBB). These agents will accumulate in areas of BBB damage or other abnormality (for instance, where there is radiation damage or brain tumor) and reduce T_1 in proportion to the concentration of free radicals. The use of paramagnetic metals, as complexes with chelating agents such as EDTA and DTPA, is also being pursued (*9, 30*). Both of these agents appear well suited for use as markers of tissue perfusion and as urographic agents, given their predominantly renal excretion pathway.

One of the more exciting frontiers in this current effort is the development of tissue-specific monoclonal antibodies labeled with paramagnetic metal ions. By using the Fab fragment of antibodies against myosin which are labeled with manganese (*33*) by means of the bifunctional chelator DTPA, selective enhancement of relaxation rates in infarcted myocardium imaged ex vivo has been observed (*34*). Since relative relaxation enhancement is increased by the large size and thus decreased correlation time (τ_c) of the ion-protein complexes, acceptably low tissue concentrations of the paramagnetic metal ion–monoclonal antibody complex are believed to be adequate. Ways to increase the number of paramagnetically labeled sites on the antibody are being sought so that this strategy can be applied to the study of other lesions (for example, tumors) with far fewer antigenic sites (*34a*).

Blood Flow

Flow effects in nonimaging NMR experiments have been known for many years (*35*). During the early application of NMR to imaging, modulation of the signal due to motion of protons (spins) in the flowing blood was noted (*23, 36*), and in vitro phantom and theoretical studies demonstrated the complex nature of the intensity increases and decreases relative to adjacent tissues (*37*). Blood flow usually decreases the signal intensity but increases can also occur. The effects arise from selectively excited spins flowing out of the image plane; fully magnetized proton spins flowing into the image plane; as well as from the phase evolution of the proton spin ensemble during flow parallel to the gradient. For an arbitrary flow direction relative to the gradient axes, the mixture of the inflow and outflow effects and phase evolution effects, if not properly understood, can lead to mistaken interpretation of the images (*38*).

In vivo Spectroscopy

If all nuclei of a particular type in a patient experienced the same static field B_0 they would all absorb energy at the same frequency. Fortunately, this is not the case. The static field induces currents in the molecular electron clouds which screen the nuclei, producing a local effective B_0 field which is slightly smaller than the applied B_0 field. The amount of reduction depends on the type of chemical bonds in the molecule, so that nuclei in different chemical environments absorb energy at different frequencies. The displacement of the resonance frequency from some chosen reference frequency is called the chemical shift. In vivo NMR spectroscopy seeks to obtain this chemical shift information for nuclei within the patient.

NMR spectroscopy is a primary tool in chemistry, and its application to living systems has been extensively reviewed (*7, 39*). Areas currently under investigation include studies of metabolism by use of ^{31}P, ^{13}C, and ^{1}H spectra. The list of nuclei that can be used for in vivo spectroscopic studies is short, because apart from hydrogen the natural abundances of nuclei with nonzero spins in the body are small (Table 2). For example, the concentration of ^{31}P in each ATP spectral line is 3 m*M*, whereas the concentration of water protons in tissue is about 90*M*.

The simplest way to obtain spectra from a patient is to place a small RF coil consisting of one or more turns of wire on the body surface near the organ of interest (*40*). The sensitive region is determined by the coil magnetic field B_1 and is limited in depth to about one coil radius. The major problems with this technique are poor localization and spectral quantitation. It is hard to tell whether a spectral peak is due to a few nuclei close to the RF coil or to many nuclei far away. This is a severe handicap in spectroscopy of the brain through the skull and scalp, and in spectroscopy of other organs as well. To address this problem, several methods have been employed to select the region of interest. Localized spectroscopic information can be obtained. For example, topical magnetic resonance (TMR) uses a B_0 field that is homogeneous over the region of interest and inhomogeneous elsewhere, allowing selection of the desired signals by some post-processing (*41*). Oscillating gradients may also be used to select sensitive planes, lines, or points (*42*). Narrow-band pulses and gradients which are switched off during data acquisition can be used for slice selection. Coils can be specially configured to give a spatial distribution of RF field strengths (*43*). Finally, the spin system can be excited with an RF pulse train in such a way that the B_1 field for 90° or 180° spin flips is remote from the RF coil (*44*). To obtain adequate signal-to-noise ratios in acceptable amounts of time, trade-offs between spatial and spectral resolution can be made. For many applications a combination of methods will probably produce the best results. For example, one might use a surface coil for its low noise performance together with pulsed gradient spatial encoding for localization and simultaneous proton imaging for definition of the region of data acquisition.

Until recently, in vivo applications of chemical shift spectroscopy were limited to small animals because of the severe demands which spectroscopy makes on magnet design: fields in excess of 1.0 T and homogeneity better than 1 part per million (ppm) in the region of interest are usually required to resolve the important resonances. For example, the interesting phosphorus resonances extend over a frequency range of 30 ppm, the resonances for ^{13}C over 200 ppm, and the resonances for the protons of biological molecules over 10 ppm. To ensure spectral line separation when surface coils are used, the homogeneity in the region of interest should be 1 ppm or less. Proton spectra from available commercial superconducting magnets with fields of 1.5 T or more are adequate to separate the water protons from those of fat. As the signal-to-noise ratio improves with field strength, there is a desire to continue increasing field strength in order to detect resonances of low intensity. However, the higher the field the greater the frequency, and the power required for penetration into the subject increases accordingly.

In the past 3 years, investigators have been able to obtain in vivo ^{31}P, ^{13}C, and ^{1}H chemical shift spectra from the body by using a 1.5- to 1.9-T superconducting magnet (*4, 5, 45*). Images of the body have been obtained at a frequency of 63 MHz with proton NMR and a 1.

magnet (*45*). Since the γ of ^{13}C is one-fourth that of protons, it should also be possible to image the body with ^{13}C by using the same frequency and a 6-T magnet, when such a magnet becomes available.

By using an indirect spin-spin double-resonance procedure one can obtain proton spectra that reflect the concentration of ^{13}C compounds. The signals of protons bonded to ^{13}C can be selectively modulated, and by this indirect method the concentrations and identity of endogenous and selectively enriched carbon compounds can be measured with a sensitivity far exceeding that of a direct ^{13}C measurement (*46*).

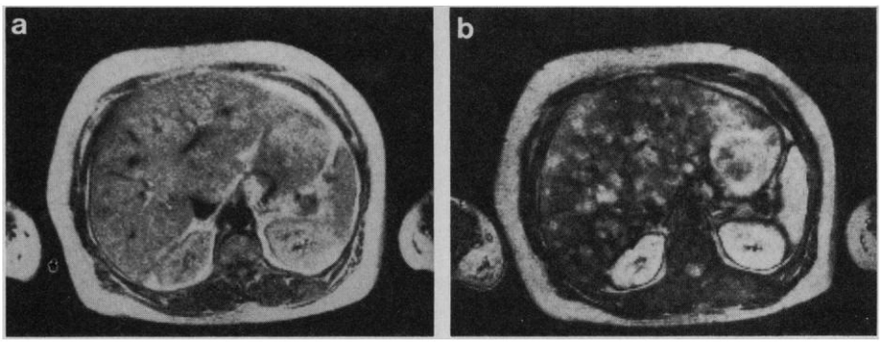

Fig. 4. Proton NMR images obtained with a spin-echo pulse sequence (40 msec TE, 1.5 second TR): (a) conventional spin-echo sequence, (b) spin-echo sequence modified so that lipid spins are 180° out of phase with water spins. [Courtesy of W. T. Dixon, Washington University (*49*)]

Spectroscopic or Chemical Shift Imaging

Spectroscopic imaging provides the spatial distribution of the concentration of some biological compound identified by its chemical shift. Chemical shift proton imaging experiments have demonstrated the two spectral peaks of water and aliphatic (CH_2) protons (*47*). This finding has already been applied to study fatty infiltration of the liver and has demonstrated a potential for quantitative determination of liver fat (*48*). Chemical shift images which show the difference between water and fat can be produced by a new technique with a resolution, imaging speed, and signal-to-noise ratio comparable to those of ordinary imaging (*49*). The method is implemented by a pulse sequence that gives water and fat signals either in phase or 180° out of phase from one another, permitting separate images of the water and fat resonances to be computed (Fig. 4).

Other techniques have been developed for acquiring chemical shift spectral data for ^{31}P from the complete array of pixels that constitute a one-dimensional, two-dimensional, or three-dimensional image (*50*). For a three-dimensional image array this means collection of four-dimensional information. Although the sensitivity of this technique is extremely low compared to that of proton NMR imaging of water and fat, the importance of the physiological information may, in many cases, justify the sacrifice in volume resolution (5 to 9000 mm^3) or data acquisition time. For example, imaging studies of phosphorus nuclei in the cat brain have demonstrated differences in the high- and low-energy phosphorus peaks in ischemic states (*51*). Unfortunately, such studies of phosphorus with current field strengths and equipment are prohibitively long (2 to 4 hours), but higher magnetic field strengths will reduce this time. Of perhaps greater significance is the possibility of imaging a host of compounds when the predominant H_2O signal is suppressed. Given the high sensitivity of protons and the favorable relaxation times (long T_2, relatively short T_1) of protons associated with amino acids and lactate, proton chemical shift imaging with solvent suppression appears promising for applications such as the study of tissue ischemia at the field strengths currently available (~1.5 T) (*51*). However, this method requires greater magnetic field homogeneity over the whole volume of the object than does conventional imaging, and this remains a significant technical hurdle.

Magnetization Transfer

It is possible to study reaction kinetics with NMR by observing the temporal changes in chemical shift spectra after RF irradiation at a resonance frequency that corresponds to the chemical shift of the nuclei in a particular chemical state.

If the chemical reactions that transfer nuclei from one chemical state to another occur in a time that is short compared to the relaxation time, the rate of transfer can be measured by observing the changes in intensity of signals caused by irradiation at specific frequencies. This technique has been applied extensively in organ studies of the creatine kinase reaction (*52*).

Clinical Applications

Central nervous system and spinal cord. Most lesions in the central nervous system (CNS) have long T_1's and T_2's compared with adjacent tissue or similar regions of the normal brain in the opposite hemisphere. Inversion recovery and saturation recovery techniques give T_1-weighted images with excellent anatomical detail. However, the T_2-weighted spin-echo technique (*53*) appears to provide the most clinically useful images of the CNS. Brain pathology is best demonstrated at present with late echoes, using long TE values, because the long T_2 of the abnormality allows its signal to remain intense while the signal from adjacent tissue decreases. Tumors (Fig. 5), infarction, hemorrhage, and demyelinating diseases give good contrast in such images because of this prolongation of T_2. Because the inherent contrast be-

Table 2. Nuclei usable for in vivo spectroscopic studies.

Element	Relative sensitivity at constant field for equal numbers of nuclei	Tissue concentration (molar)	Relative detection sensitivity
^{1}H	1.0	90*	1.0
^{19}F	0.83	2.6†	2.4×10^{-2}
^{23}Na	0.09	0.14‡	1.4×10^{-4}
^{31}P	0.07	0.008§	6.2×10^{-6}
^{13}C (storage lipid)	0.016	0.45‖	8.0×10^{-5}
^{13}C (endogenous lactate)	0.016	0.00005¶	8.9×10^{-9}**

*Hydrogen from 80 percent water in tissues. †Blood concentration after injection of 500 ml of fluorocarbon. ‡Blood and extracellular fluid. §Concentration of tissue phosphorus associated with ATP or creatine phosphate. ‖Assuming 7.3 mg of ^{13}C per gram of adipose fat tissue at the natural abundance of 1.1 percent ^{13}C. ¶Natural abundance of ^{13}C for a lactate concentration of 5 m*M*. (^{13}C-methyl is 0.05 m*M*). **Theoretically, 60 times greater relative sensitivity can be achieved by spin-spin heteronuclear double-resonance techniques. Presently achieved threshold for detection of enriched ^{13}C-lactate in vivo is 0.5 m*M* per minute (*46*). Proton spectroscopy using homonuclear double-resonance techniques or spin-echo methods is capable of detecting endogenous lactate at normal and pathological concentrations.

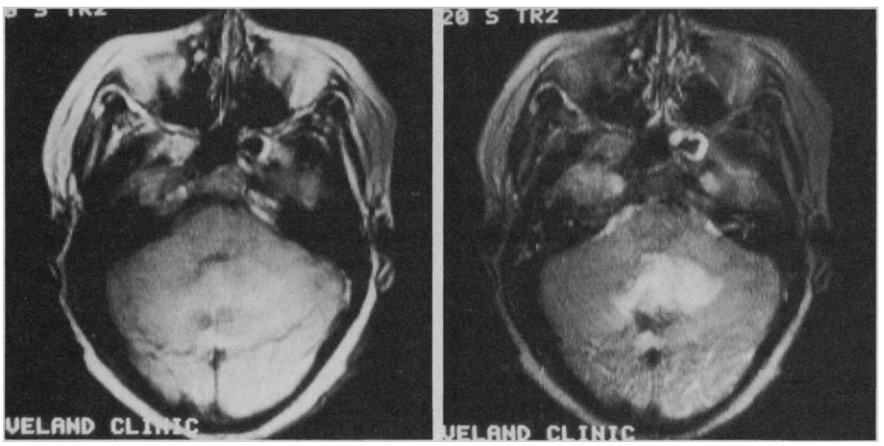

Fig. 5. Proton NMR images demonstrate the dependence of the contrast between abnormal and normal tissues on the timing of the 180° RF pulse intervals for spin-echo imaging. The pulse sequence interval (TR) was 2000 msec and the TE was 30 msec (left) and 120 msec (right). The T_2 of tumor is longer than that of normal tissue, so that as long as there is an adequate signal-to-noise ratio, the longer TE corresponds to greater contrast, in accord with Eq. 1 and Fig. 2. [Courtesy of M. Weinstein and T. F. Meaney, Cleveland Clinic]

tween normal and abnormal tissues is much greater with NMR than with x-ray CT, small lesions in white matter, such as the plaques of multiple sclerosis and the patches of periventricular demyelination noted in aging, are detected readily by NMR (*54*). Improvements in spatial resolution and multienergy capabilities of x-ray CT instrumentation may, however, narrow the gap of NMR superiority. Although the presence of a tumor is reliably detected with NMR, the extent of the tumor is frequently difficult to ascertain because of the similarity of the signal from surrounding edematous brain.

Disease of the spinal cord is best defined by sagittal plane NMR imaging (Fig. 6). Surface coils have recently been employed to provide improved image quality for the brain and spinal cord (*55*). The excitation pulse is provided by a large coil that surrounds the head or body, and signals are detected by a small coil applied near or on the body surface, adjacent to the region of interest.

NMR imaging of the central nervous system and spinal cord has high sensitivity for disease detection, but the specificity of differentiation of disease categories has been less than hoped for. NMR does not detect a signal from calcium deposits and in general has somewhat less resolution than the best x-ray CT scanners. Further, NMR does not have the sensitivity to describe glucose metabolic rate, neurotransmitter concentration, or amino acid transport with the spatial resolution of emission tomography. Nevertheless, proton NMR of the CNS provides detailed anatomic information in any desired plane, without the artifacts which degrade x-ray CT image information near bony structures.

In vivo spectroscopic study of the infant brain is a new method for determining prognosis and selecting therapy (*55a*).

Thorax and lungs. Proton NMR has shown less potential in the thorax than in other areas of the body. The reasons are low signal strength from the lungs and motion caused by breathing and the pulsation of the great vessels. The signal from the lungs is low because the proton density is about 10 to 35 percent of that in soft tissue.

The low signal of flowing blood does, however, have the advantage of delineating the lumina of the major vessels. X-ray CT can demonstrate airways and pulmonary vessels well, with far fewer artifacts and less blurring from motion, because x-ray CT imaging is faster and has higher spatial resolution than NMR. Small nodules can be missed in NMR images because of blurring of the signal due to the poor in-plane resolution and the partial volume effect when slices of 7 mm or greater are used. Calcification, which is especially helpful in identifying nodules on x-ray images, is not seen.

Spin-echo images, obtained with both a long repetition time of 1 to 2 seconds and a short repetition time of 0.5 second, can be used to separate mediastinal tumors from mediastinal fat (*56*). Inversion recovery images can also separate tumor from fat. Because of the absence of a signal from flowing blood and the ability to separate mediastinal tumor from soft tissues (*44*), NMR can provide unique information which is complementary to that of x-ray CT and arteriography. For example, large hilar masses can easily be distinguished from hilar vessels with NMR because the vessel lumina are well defined by the absence of a signal from flowing blood (*56*).

A major theoretical potential of NMR is in the quantitation of lung water. A new method for distinguishing lung water in aerated lungs from that in nonaerated lungs has been described (*57*). The method is based on microscopic changes in magnetic field homogeneity which arise from the difference in magnetic susceptibilities of air and water. Special pulse and gradient sequences can be used to evaluate this phenomenon in inflated and noninflated lung.

Cardiac imaging. Rapidly flowing blood can be made to give a weak NMR signal and the cardiac chambers and greater vessels may appear as low-intensity regions, in marked contrast to myocardium and vessel walls. By timing the image sequence relative to the cardiac cycle (gating), images with good contrast resolution and excellent spatial resolution are obtained without the use of injected contrast material (*58*). These images demonstrate the thickness and homogeneity of myocardial and vessel walls, as well as the sizes of their lumina. Chamber and vessel size can be determined and images from different time periods in the cardiac cycle can be obtained to provide, in principle, physiological information similar to that from gated blood pool imaging in nuclear medicine, as well as information on wall thicknesses, which is now usually obtained with ultrasound. At present, gated proton NMR cardiac studies require long acquisition times. For many clinical applications, ultrasound, x-ray CT, and nuclear medicine procedures are more practical, and provide similar anatomic and functional information. The unique potentials of NMR appear at present to be in the detection of inflammatory disease of the pericardium and ischemic heart disease, through relaxation parameter changes (*59*).

Atherosclerotic lesions can be detected from distortion of vessel lumina. The low intensity usually associated with flow provides the contrast necessary to detect abnormalities in vessel walls (*37, 60*). Interpretation of signals from arterial wall tissue is difficult because calcium and cholesterol give no signal, while clotted and fibrous tissue deposits give a signal whose intensity varies with composition. Blood flow abnormalities around arterial wall irregularities can lead to paradoxical signals which depend on velocity, turbulence, gradient directions, and pulse sequences (*38*). Nevertheless, the noninvasive nature of NMR and its ability to characterize tissue

make NMR imaging an important new tool for the study of arterial wall disease from childhood through adulthood.

Peripheral vessel disease can be detected indirectly by in vivo spectroscopic measurement of altered muscle metabolism (*60a*).

Breast imaging. While hopes are high for proton NMR as a noninvasive imaging mode for breast disease, progress has been disappointing. A few important clinical studies are under way (*61*). Once the RF coil design and human engineering problems have been worked out, NMR proton imaging of the breast might be an extremely important clinical procedure. Surface coil imaging is a logical extension of previous work.

Abdominal imaging. Proton NMR is being evaluated for imaging the abdomen. The solid portions of the liver and spleen give relatively homogeneous signals, with the vessels outlined because of the low or absent signals from regions of flowing blood. Abnormalities in these organs, due to tumor or metabolic disease, are usually characterized by prolongation of T_1 and T_2 (*62*). To take advantage of this, spin-echo pulse sequences are typically repeated every 1.5 seconds and data are examined for an echo delay of 40 msec or longer. With this sequence most tumors and focal abnormalities are seen as high-intensity areas, which are well delineated from normal liver and splenic tissue (Fig. 7).

Inversion recovery (Fig. 2) can demonstrate the prolonged T_1 of liver and spleen tumors if the inversion delay is chosen properly. If the TI is chosen so that the normal tissue gives no signal (this occurs when TI is 0.693 T_1 and TR $\gg T_1$), then any area of intensity represents an abnormality and may be due to either longer or shorter T_1 (Fig. 7).

The gallbladder can be successfully evaluated by using pulse sequences with short TE to emphasize regions of short T_2. The intensity of the signal varies directly with the concentration of bile (*63*). Function can be evaluated by the changes in bile concentration produced by fasting and postprandial states. Gallstones appear as filling defects because they emit virtually no signal.

NMR proton imaging of the pancreas is less promising because of its poorer resolution compared to x-ray CT, motion blurring, and difficulties in separating pancreas from bowel.

The gastrointestinal tract has, thus far, been difficult to image because of the motion of peristalsis and respiration, the lack of adequate spatial resolution, and the lack of sufficient contrast difference between bowel wall and surrounding

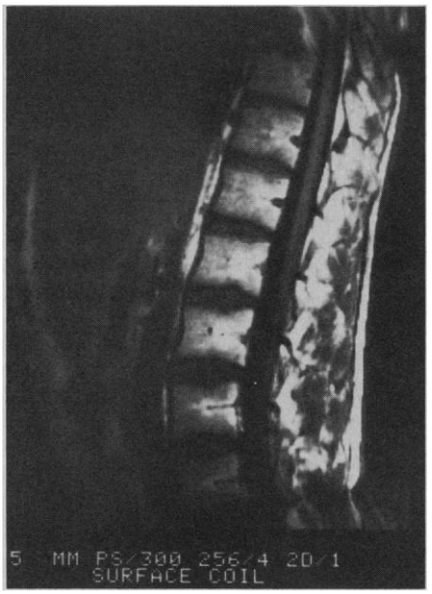

Fig. 6. Sagittal section, 5 mm thick, of the normal spinal cord and canal imaged with surface coil techniques at 1.5 T and partial saturation with a repetition time of 0.3 second. [Courtesy of J. Schenck and co-workers (*55*)]

structures. Use of oral contrast media may greatly facilitate NMR of the gastrointestinal tract; however, more conventional methods of examination of the gastrointestinal tract provide information that is not available with present NMR technology.

Genitourinary imaging. Proton NMR is well suited to examination of the kidneys and of the organs of the male and female pelvis because it clearly separates adjacent fat and soft-tissue planes (*64*). The renal cortex, medulla, hilum, and vessels can be demonstrated better by NMR than by any other noninvasive imaging method. The vessels appear with low intensity because of the lack of signal from flowing blood. The renal hilum, which contains a large amount of fat, gives an intense signal, and the cortex and medulla have greatly different T_1's (the T_1 of the medulla is longer) and are easily separated by spin-echo or inversion recovery imaging. Appropriate T_2 characterization, using early or late spin echoes, can give accurate identification of fat, cystic lesions, and renal parenchymal disease, in which increased water content leads to a prolongation of T_2.

NMR of the pelvis can provide clear separation of the normal structures. In T_2-enhanced spin-echo images, muscles, vessels, and lymph nodes are easily separated from adjacent pelvic organs, particularly if axial, sagittal, and coronal planes are routinely generated. When specific abnormalities are sought, the imaging technique can be selected to maximize detection; for example, lymph nodes can best be separated from fat by T_2-weighted images with a short TR interval (0.5 second). The uterus is best imaged by a long TR (1.5 seconds) and late echoes (long TE) because the myo-

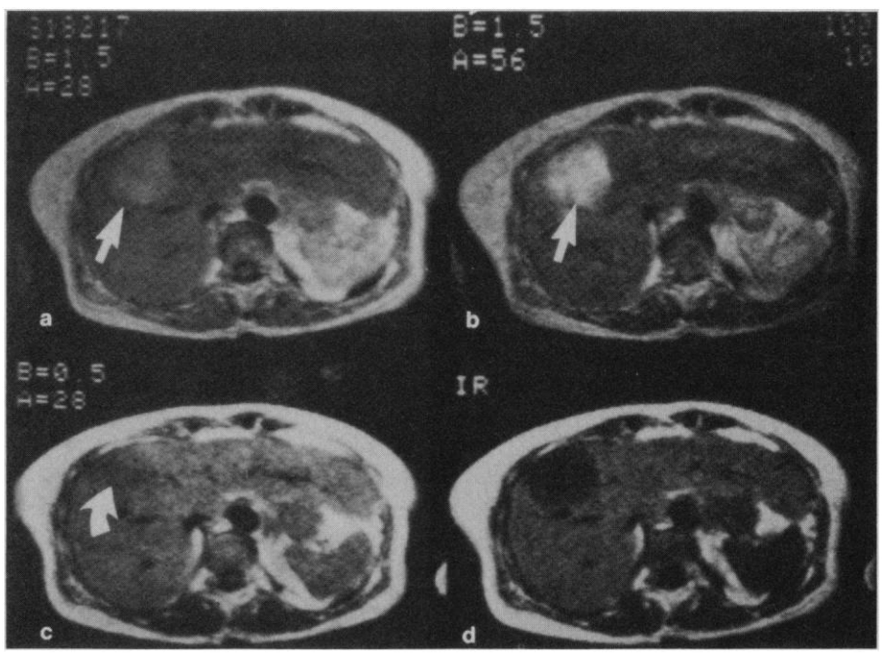

Fig. 7. Hepatic metastasis. Spin-echo images: (a) 1.5 seconds (TR) and 28 msec (TE); (b) 1.5 seconds and 56 msec; (c) 0.5 second and 28 msec. (d) Inversion recovery image. The metastasis (arrows) appears as a region of increased intensity in (a) and (b) and as a mass of slightly lower intensity (curved arrow in c). The metastasis has very low intensity in the inversion recovery image (see Eq. 1 and Fig. 2). [Courtesy of A. R. Margulis, L. Kaufman, and L. E. Crooks, Radiological Imaging Laboratory, University of California]

metrium has a longer T_2 than the endometrium. In general, pelvic tumors are characterized by long T_2 relaxation times and are best demonstrated with late spin-echoes.

Musculoskeletal imaging. A general feature of NMR imaging that makes it well suited for a number of musculoskeletal applications is its soft-tissue contrast, which is superior to that of x-ray CT (*65*). Fat, muscle, fibrous structures, nerves, and blood vessels have different NMR imaging characteristics, but, with the exception of fat, have very similar CT attenuation values. A disadvantage of NMR at present is its poor spatial resolution compared to that of x-ray CT and conventional x-ray imaging of the back.

Compact bone appears dark and is surrounded by signals that reflect the T_1 and T_2 of soft tissues and of yellow marrow, which has a high fat content. Intervertebral disk disease can be evaluated in a new way by NMR. Nuclear magnetic resonance usually differentiates between two parts of the intervertebral disk—the nucleus pulposus from the annulus fibrosis—while x-ray CT cannot make this distinction. Because of the relation of T_2 to hydration of the vertebral disk, NMR is extremely sensitive for the detection of degeneration (*66*). In most patients with disk disease, the involved disks show loss of the normal high-intensity signal from the nucleus pulposus, and it seems likely that NMR may demonstrate abnormalities in disk material even in the absence of overall anatomic derangement, such as herniation. In addition, the NMR signal is distinctive for avascular necrosis of the femoral head. Because of the superior soft-tissue contrast of NMR, abnormal growths and pathological derangements in and around bone are also readily detected. A very high resolution NMR image of the spinal cord and vertebrae in a normal human subject was recently obtained by using a surface coil (Fig. 6).

Detection of congenital abnormalities in muscle metabolism by in vivo spectroscopy is a unique capability of ^{31}P NMR (*66a*).

Safety of NMR

Experimental studies of the effects of static magnetic fields on biological systems have not revealed effects that could be harmful to human health at fields up to 2 T, the limit of most studies (*67*). Effects on bacterium orientation and animal navigation and the induction of potentials due to blood flowing in the field are not considered biologically harmful. Reports of experimental results showing possible harmful effects in systems ranging from enzyme-controlled reactions to temperature changes in small animals continue to appear in the literature. Analysis of these experiments usually reveal a lack of control for mechanical or sonic frequency vibrations, specimen or preparation handling, or temperature and ambient light (*67*).

Clinical studies involving fields beyond 2 T will require an extension of safety studies, although at present there is no evidence from ^{31}P spectroscopic studies in vivo that metabolism is affected by magnetic fields. Although charge separation, conformational, and orientational changes in molecules or assemblages of molecules and magnetohydrodynamic effects can occur, their magnitude and importance at fields anticipated in the near future (4 to 6 T) have yet to be ascertained.

Radio frequencies required will result in some body heating, whose magnitude will be dependent on frequency, pulse timing, configuration of the RF probe, body mass in the RF probe, and the ability of the body to lose heat. As field strength increases the amount of power required for an effective 90° or 180° pulse increases because of body absorption, increasing body heating.

Proton imaging systems operating at fields up to 0.6 T have not been found to cause any temperature elevation in the living human. At fields of 1.5 T (63 MHz), phantoms simulating the human torso in configuration and conductivity can be heated, but the ability of the body to lose heat must be included in future evaluations of the significance of these elevations. Imaging techniques (for example, number of slices) and pulse sequences can be chosen to limit temperature elevation, although there will be a concomitant increase in imaging time or loss in resolution. Core temperature elevations less than 1°C might be considered safe; however, guidelines for the routine practice of NMR proton imaging are not yet firmly established (*68*).

A third area of possible hazard involves currents induced by rapidly changing gradients used to acquire spatial information. A change in magnetic field will induce a current in proportion to the orientation, radius, and conductivity of the current path associated with the field change. Both the rate of change and the duration of the change must be taken into account, and the expected response is analogous to the voltage-duration relations in nerve stimulation. Visual phosphenes (*69*) can be stimulated by a change in field of 1.3 T/sec and a pulse rise time of 2 msec. Gradient field changes in NMR systems are as rapid, but have a shorter duration. Even though visual phosphenes might be generated by the NMR systems of the future, no known biological hazard has been recognized from pressure, electrical, or magnetic visual phosphenes. The currents required for nerve stimulation are orders of magnitude greater than those required for induction of phosphenes (*67, 70*). The medical community will need to be alert to other effects of rapid field changes yet to be discovered.

The known hazards of NMR are due to the force and torque exerted by the field on ferromagnetic objects brought into the vicinity of the magnet and on patients' prostheses such as surgical clips, pacemakers, and joint replacements. Each category of protheses requires an evaluation at different field strengths for a risk-benefit assessment (*71*). High fields which are known in the environment range from 1.2 mT (12 gauss) at human waist level on loaded electric transport systems under acceleration (*72*) to 4.0 mT (40 gauss) in aluminum reduction plant facilities. At fields of 1 to 2 mT the reed switch of cardiac pacemakers might be activated and some electronic equipment might be affected, so that control of equipment and personnel traffic near the magnets is common practice.

Conclusions

Proton (hydrogen) NMR is now a well-established noninvasive imaging technique which gives better contrast and sensitivity than does x-ray CT. This has now been demonstrated in the brain and pelvis, and there are important clinical applications for other regions, particularly for cardiovascular and musculoskeletal problems.

Proton imaging techniques, including data acquisition and processing, continue to be refined to give better resolution, signal-to-noise ratio, and contrast. Cardiac and respiratory gating have given clearer images of the thorax and abdomen, and surface coil imaging methods now permit very high resolution of, for example, the orbit and selected regions of the spine.

In vivo spectroscopy has already provided a new tool for investigation of metabolism, and new imaging techniques make it possible to determine the region-

al distribution of spectroscopically identifiable metabolites. This improvement over previous selected-region spectroscopic methods has been a result of innovations in pulse sequence encoding techniques, signal processing procedures, and magnetic field homogeneity.

References and Notes

1. E. Odeblad, B. Bhar, G. Lindstrom, *Arch. Biochem. Biophys.* **63**, 221 (1956); C. B. Bratton, thesis, Case Western Reserve University (1964); ———, A. L. Hopkins, J. W. Weinberg, *Science* **147**, 738 (1965); T. R. Ligon, M. S. thesis, Oklahoma State University (1967); J. A. Jackson and W. H. Langham, *Rev. Sci. Instrum.* **39**, 510 (1968).
2. R. Damadian, *Science* **171**, 1151 (1971).
3. P. C. Lauterbur, *Bull. Am. Phys. Soc.* **18**, 86 (1972); *Nature (London)* **242**, 190 (1973).
4. R. B. Moon and H. J. Richards, *J. Biol. Chem.* **248**, 7276 (1973); D. I. Hoult *et al.*, *Nature (London)* **252**, 285 (1974); B. Chance, Y. Nakase, M. Bond, J. S. Leigh, Jr., G. McDonald, *Proc. Natl. Acad. Sci. U.S.A.* **75**, 4925 (1978); D. P. Hollis *et al.*, *J. Magn. Reson.* **29**, 319 (1978); R. L. Nunnally and P. A. Bottomley, *Science* **211**, 177 (1981); B. D. Ross *et al.*, *N. Engl. J. Med.* **304**, 1338 (1981); R. H. T. Edwards, M. J. Dawson, D. R. Wilkie, R. E. Gordon, D. Shaw, *Lancet* **1982-I**, 725 (1982); E. B. Cady *et al.*, *ibid.* **1983-I**, 1059 (1983).
5. J. R. Alger *et al.*, *Science* **214**, 660 (1981); K. L. Behar *et al.*, *Proc. Natl. Acad, Sci. U.S.A.* **80**, 4945 (1983); K. J. Neurohr, E. J. Barrett, R. G. Shulman, *ibid.*, p. 1603; J. W. Prichard *et al.*, *ibid.*, p. 2748; P. A. Bottomley *et al.*, *Radiology* **150**, 441 (1984); M. J. Dawson, in *Cardiac Metabolism*, A. J. Drake-Holland and M. I. M. Noble, Eds. (Wiley, New York, 1983).
6. C. Green and A. Suttle, Eds., *National Conference on Biomedical Engineering. NMR Clinical Aspects* (National Academy Press, Washington, D.C., in press).
7. A. Abragam, *Principles of Nuclear Magnetism* (Oxford, London, 1983); E. D. Becker, *High Resolution NMR* (Academic Press, New York ed. 2, 1980), pp. 184–275; C. P. Slichter, in (*32*); P. Mansfield and P. G. Morris, *NMR Imaging in Biomedicine* (Academic Press, New York, 1982); D. G. Gadian, *Nuclear Magnetic Resonance and Its Applications to Living Systems* (Clarendon, Oxford, 1982); C. L. Partain, A. E. James, F. D. Rollo, R. R. Price, *Nuclear Magnetic Resonance Imaging* (Saunders, Philadelphia, 1983); I. L. Pykett, *Sci. Am.* **246**, 78 (May 1982); A. R. Margulis, C. B. Higgins, L. Kaufman, L. E. Crooks, *Clinical Magnetic Resonance Imaging* (Radiology Research and Education Foundation, San Francisco, 1983); T. L. James and A. R. Margolis, Eds., *Biomedical Magnetic Resonance* (Radiology Research and Education Foundation, San Francisco, 1984).
8. S. H. Koenig and W. E. Schillinger, *J. Biol. Chem.* **244**, 3283 (1969); K. Hallenga and S. H. Koenig, *Biochemistry* **15**, 4255 (1976).
9. A short review with numerous references is given by S. H. Koenig and R. D. Brown III, *Magn. Reson. Med.*, in press.
10. S. H. Koenig, R. D. Brown III, D. Adams, D. Emerson, C. G. Harrison, *Invest. Radiol.* **19**, 76 (1984); S. H. Koenig and R. D. Brown III, *Magn. Reson. Med.*, in press.
11. B. M. Fung and P. S. Puon, *Biophys. J.* **33**, 27 (1981); D. P. Hollis, L. A. Saryan, H. P. Morris, *Johns Hopkins Med. J.* **131**, 441 (1972); C. L. Hazlewood, *J. Natl. Cancer Inst.* **52**, 625 (1974); ———, B. L. Nichols, N. F. Chamberlain, *Nature (London)* **222**, 747 (1969); W. R. Inch, J. A. McCredie, R. R. Knispel, R. T. Thompson, M. M. Pintar, *J. Natl. Cancer Inst.* **52**, 353 (1974); K. R. Foster, H. A. Resing, A. N. Garroway, *Science* **194**, 324 (1976); R. Mathur-DeVre, *Prog. Biophys. Mol. Biol.* **35**, 103 (1979); G. N. Ling and M. Tucker, *J. Natl. Cancer Inst.* **5**, 1199 (1980); G. D. Fullerton, J. L. Potter, N. C. Dornbluth, *Magn. Reson. Imaging* **1**, 209 (1982); P. L. Beall, C. F. Hazlewood, P. N. Rao, *Science* **192**, 904 (1976).
12. S. H. Koenig, *ACS Symp. Ser. No. 127* (1980), p. 157.
13. P. L. Davis, L. Kaufman, L. E. Crooks, in *Nuclear Magnetic Resonance Imaging in Medicine*, A. R. Margulis, L. Kaufman, L. E. Crooks, Eds. (Radiology Research and Education Foundation, San Francisco, 1982), p. 53; I. L. Pykett, B. R. Rosen, F. S. Buonanno, T. J. Brady, *Phys. Med. Biol.* **28**, 723 (1983); L. E. Crooks *et al.*, *Radiology* **146**, 123 (1983); T. J. Brady *et al.*, *Am. J. Neuroradiol.* **4**, 225 (1983); M. S. Lin, *Magn. Reson. Med.* **1**, 361 (1984).
14. D. A. Ortendahl, N. M. Hylton, L. Kaufman, L. E. Crooks, *Magn. Reson. Med.* **1**, 316 (1984). The equation is correct if TR > 0.5 second and T_2 < 200 msec. See also W. A. Edelstein, P. A. Bottomley, H. R. Hart, L. S. Smith, *J. Comput. Assist. Tomogr.* **7** (No. 3), 391 (1983); F. W. Wehrli *et al.*, *ibid.* **8** (No. 3), 369 (1984).
15. Spin echo is an NMR technique in which a 180° RF pulse (or a reversal of the gradient field) is applied after the 90° RF pulse. The reappearance of an NMR signal is a result of the effective reversal of the dephasing of the spins ("refocusing"). The 180° pulse is applied after a time shorter than or on the order of T_2. Multiple spin echoes or a series of spin echoes at different times can be used to determine T_2 without effects of the inhomogeneity of the magnetic field. Inversion recovery is an NMR technique in which the nuclear magnetization is inverted by a 180° RF pulse and after a time interval (TI) the partial relaxation of the spins, which depends strongly on T_1, is measured, usually by a 90° to 180° spin-echo RF pulse sequence. The T_1 in a given region can be calculated from the change in the NMR signal due to the inversion pulse compared to the signal with no inversion pulse or an inversion pulse with a different inversion time (TI).
16. G. E. Wesbey, M. E. Mosley, R. L. Ehman, *Invest. Radiol.*, in press.
17. W. S. Hinshaw, *J. Appl. Phys.* **47**, 3709 (1976); P. Mansfield and P. G. Morris, *NMR Imaging in Biomedicine* (Academic Press, New York, 1982).
18. R. Damadian, L. Minkoff, M. Goldsmith, J. A. Koutcher, *Naturwissenschaften* **65**, 250 (1978); R. Damadian *et al.*, *Science* **194**, 1430 (1976).
19. A. N. Garroway, P. K. Grannell, P. Mansfield, *J. Phys. C* **7**, 457 (1974); L. E. Crooks, M. Arakawa, J. Hoenninger, *Radiology* **143**, 169 (1982).
20. P. C. Lauterbur and C.-M. Lai, *IEEE Trans. Nucl. Sci.* **NS-27**, 1227 (1980).
21. P. Brunner and R. R. Ernst, *J. Magn. Reson.* **33**, 83 (1979); C. M. Lai and P. C. Lauterbur, *Phys. Med. Biol.* **26**, 851 (1981).
22. A. Kumar, D. Welti, R. R. Ernst, *J. Magn. Reson.* **18**, 69 (1975).
23. W. A. Edelstein, J. Hutchsinon, G. Johnson, T. Redpath, *Phys. Med. Biol.* **25**, 751 (1980).
24. P. Mansfield, *J. Phys. Solid State C* **10**, L55 (1977); ——— and I. L. Pykett, *J. Magn. Reson.* **29**, 355 (1978).
25. T. R. Brown, B. M. Kincaid, K. Ugurbil, *Proc. Natl. Acad. Sci. U.S.A.* **79**, 3523 (1982); D. B. Twieg, *Med. Phys.* **10**, 610 (1983); S. J. Ljunggren, *J. Magn. Reson.* **54**, 338 (1983); K. F. King and P. R. Moran, *Med. Phys.* **11**, 1 (1984); R. B. Marr, "Linear methods in magnetic resonance imaging" (Applied Mathematics Department Report 945, Brookhaven National Laboratory, 1984).
26. D. I. Hoult, *J. Magn. Reson.* **33**, 183 (1979).
27. ——— and P. C. Lauterbur, *ibid.* **34**, 425 (1979); D. I. Hoult and R. E. Richards, *ibid.* **24**, 71 (1976).
28. P. A. Bottomley *et al.*, *Radiology* **150**, 441 (1984).
29. L. E. Crooks *et al.*, *ibid.* **151**, 127 (1984).
30. D. I. Hoult, in *Biomedical Magnetic Resonance*, T. L. James and A. R. Margulis, Eds. (Radiology Research and Education Foundation, San Francisco, 1984), pp. 35–45; P. C. Lauterbur, M. H. M. Dias, A. M. Rudin, in *Frontiers of Biological Energetics*, P. L. Dutton, J. S. Leigh, A. Scarpa, Eds. (Academic Press, New York, 1978), p. 752; R. C. Brasch, *Radiology* **147**, 781 (1983); M. H. Mendonca-Dias, E. Gaggelli, P. C. Lauterbur, *Semin. Nucl. Med.* **13**, 364 (1983); Y. S. Kang, J. C. Gore, I. M. Armitage, *Magn. Reson. Med.* **1**, 396 (1984).
31. R. C. Brasch *et al.*, *Radiology* **147**, 773 (1983); V. M. Runge *et al.*, *ibid.*, p. 789; R. C. Brasch *et al.*, *Am. J. Radiol.* **141**, 1019 (1983).
32. C. P. Slichter, *Principles of Magnetic Resonance* (Springer-Verlag, New York, ed. 2, 1978).
33. B. A. Khaw *et al.*, paper presented at the American Heart Association Annual Meeting, Anaheim, California, November 1983.
34. T. J. Brady *et al.*, *Magn. Reson. Med.* **1**, 230 (1984).

34a. T. J. Brady, personal communication.

35. G. Suryan, *Proc. Ind. Acad. Sci. Sect. A* **33**, 107 (1951); J. R. Singer, *Science* **130**, 1652 (1959); J. R. Battocletti *et al.*, *Proc. IEEE* **67**, 1359 (1979).
36. W. S. Hinshaw, E. R. Andrew, P. A. Bottomley, G. N. Holland, W. S. Moore, B. S. Worthington, *Neuroradiology* **16**, 607 (1978).
37. L. Kaufman, L. E. Crooks, P. E. Sheldon, W. Rowland, T. Miller, *Invest. Radiol.* **17**, 554 (1982); L. Kaufman *et al.*, *Circulation* **67**, 251 (1983); S. X. Salles-Cunha, E. Halbach, J. H. Battocletti, A. Sances, *Med. Phys.* **8**, 452 (1981); J. R. Singer and L. E. Crooks, *Science* **221**, 654 (1983); D. A. Fineberg, *Magn. Reson. Med.* **1**, 151 (1984).
38. C. R. George *et al.*, *Radiology* **151**, 421 (1984).
39. T. L. James, *Nuclear Magnetic Resonance in Biochemistry: Principles and Applications* (Academic Press, New York, 1975); R. G. Shulman *et al.*, *Science* **205**, 160 (1979); R. G. Shulman, *Sci. Am.* **248**, 86 (January 1983); O. Jardetzky and G. C. K. Roberts, *NMR in Molecular Biology* (Academic Press, New York, 1981).
40. J. J. H. Ackerman *et al.*, *Nature (London)* **283**, 167 (1980); R. E. Gordon *et al.*, *ibid.* **287**, 736 (1980).
41. R. E. Gordon, P. E. Hanley, D. Shaw, *Prog. Nucl. Magn. Reson. Spectrosc.* **15**, 1 (1982).
42. K. N. Scott, H. R. Brooker, J. R. Fitzsimmons, H. F. Bennett, R. C. Mick, *J. Magn. Reson.* **50**, 339 (1982).
43. M. R. Bendall, in *Biomedical Magnetic Resonance*, T. L. James and A. R. Margulis, Eds. (Radiology Research and Education Foundation, San Francisco, 1984), pp. 99–126; M. S. Roos, A. Hasenfeld, M. R. Bendall, R. H. Huesman, T. F. Budinger, paper presented at the 3rd Annual Meeting, Society of Magnetic Resonance in Medicine, New York, August 1984.
44. M. R. Bendall and R. E. Gordon, *J. Magn. Reson.* **53**, 365 (1983); R. Tycko, *Phys. Rev. Lett.* **51**, 775 (1983); D. Hasenfeld, paper presented at the 3rd Annual Meeting, Society of Magnetic Resonance in Medicine, New York, August 1984.
45. P. A. Bottomley *et al.*, *Radiology* **150**, 441 (1984).
46. D. L. Rothman, K. L. Behar, H. P. Hetherington, R. G. Shulman, *Proc. Natl. Acad. Sci. U.S.A.*, in press; R. Rothman *et al.*, *J. Magn. Reson.*, in press; J. A. denHollander, K. L. Behar, R. G. Shulman, *J. Magn. Reson.* **57**, 311 (1984); R. Rothman, personal communication; K. Behar, personal communication; K. Ugurbil *et al.*, *FEBS Lett.* **167**, 73 (1984).
47. I. L. Pykett and B. R. Rosen, *Radiology* **149**, 197 (1983); B. R. Rosen, I. L. Pykett, T. J. Brady, E. Carter, J. Wands, *Magn. Reson. Med.* **1**, 239 (1984).
48. J. K. T. Lee, W. T. Dixon, D. Ling, R. G. Levitt, W. A. Murphy, Jr., *Radiology*, in press.
49. W. T. Dixon, *ibid.*, in press.
50. S. J. Cox and P. Styles, *J. Magn. Reson.* **40**, 209 (1980); T. R. Brown, B. M. Kincaid, K. Ugurbil, *Proc. Natl. Acad. Sci. U.S.A.* **79**, 3523 (1982); A. A. Maudsley *et al.*, *J. Magn. Reson.* **51**, 147 (1983); J. C. Haselgrove, V. H. Subramanian, J. S. Leigh, Jr., L. Gyulai, B. Chance, *Science* **220**, 1170 (1983); P. Bendel, C. M. Lai, P. C. Lauterbur, *J. Magn. Reson.* **38**, 343 (1980); P. Mansfield, *Magn. Reson. Med.* **1**, 370 (1984).
51. B. R. Rosen, D. Wedeen, T. J. Brady, *J. Comput. Assist. Tomogr.*, in press. For phosphorus chemical shift imaging, see S. K. Hilal, A. A. Maudsley, H. E. Simon, S. Wittekoek, paper presented at the 69th Scientific Assembly and Annual Meeting, Radiological Society of North America, Chicago, November, 1983.
52. J. S. Ingwall, *Am. J. Physiol.* **242**, H729 (1982); A. P. Koretsky and M. W. Weiner, in *Biomedical Magnetic Resonance*, T. L. James and A. R. Margulis, Eds. (Radiology Research and Education Foundation, San Francisco, 1984), pp. 209–230.
53. L. E. Crooks *et al.*, *Radiology* **144**, 843 (1982).
54. I. R. Young, A. S. Hall, C. A. Pallis, M. J. Legg, G. M. Bydder, R. E. Steiner, *Lancet* **1981-II**, 1063 (1981); G. M. Bydder, J. M. Pennock, R. E. Steiner, J. S. Orr, D. A. Bailes, I. R. Young, *Magn. Reson. Med.* **1**, 5 (1984); M. Brant-Zawadzki *et al.*, *Am. J. Neuroradiol.* **4**, 117 (1983); G. M. Bydder *et al.*, *ibid.* **3**, 459 (1982); W. G. Bradley, V. Waluch, L. Brant-Zawadzki, R. A. Yadley, R. R. Wycoff, *Noninvasive Med. Imaging* **1**, 35 (1984).
55. J. Schenck *et al.*, *Am. J. Neuroradiol.*, in press.

55a. See E. B. Cady *et al.*, in (*4*).

56. W. R. Webb and G. Gamsu, in *Clinical Magnetic Resonance Imaging*, A. R. Margulis, C. B. Higgins, L. Kaufman, L. E. Crooks, Eds. (Radiology Research and Education Foundation, San Francisco, 1983), pp. 145–158; G. Gamsu *et al.*, *Radiology* **147**, 473 (1983).
57. C. E. Hayes *et al.*, *Science* **216**, 1313 (1982); D. C. Ailion *et al.*, *Bull. Magn. Reson.*, in press.

58. R. J. Alfidi *et al.*, *Radiology* **143**, 175 (1982); C. B. Higgins, R. Herfkens, M. J. Lipton, R. P. Sievers, P. Sheldon, L. Kaufman, *Am. J. Cardiol.* **52**, 184 (1983); P. Lanzer *et al.*, *Radiology* **150**, 121 (1984).
59. E. S. Williams *et al.*, *J. Nucl. Med.* **21**, 449 (1980); T. J. Brady *et al.*, *Radiology* **144**, 343 (1982); C. B. Higgins *et al.*, *Circulation* **69**, 523 (1984); C. B. Higgins, in *Biomedical Magnetic Resonance*, T. L. James and A. R. Margulis, Eds. (Radiology Research and Education Foundation, San Francisco, 1984), pp. 331–348; G. M. Pohost and A. V. Ratner, *J. Am. Med. Assoc.* **251**, 1304 (1984).
60. R. J. Herfkens *et al.*, *Radiology* **147**, 749 (1983); *ibid.* **148**, 161 (1983).
60a. B. Chance, in *Biomedical Magnetic Resonance*, T. L. James and A. R. Margulis, Eds. (Radiology Research and Education Foundation, San Francisco, 1984), pp. 187–199; D. L. Arnold, P. M. Mathews, G. K. Radda, *Magn. Reson. Med.* **1**, 307 (1984).
61. D. Medina *et al.*, *J. Natl. Cancer Inst.* **54**, 813 (1975); R. J. Ross, W. S. Thompson, C. Kim, D. A. Bailey, *Radiology* **143**, 195 (1982); S. J. El Yousef *et al.*, *J. Comput. Assist. Tomogr.* **7**, 215 (1983).
62. F. H. Doyle *et al.*, *Am. J. Radiol.* **138**, 193 (1982); A. A. Moss, D. D. Stark, H. I. Goldberg, A. R. Margulis, in *Clinical Magnetic Resonance Imaging*, A. R. Margulis *et al.*, Eds. (Radiology Research and Education Foundation, San Francisco, 1983), pp. 185–207.
63. H. Hricak, R. A. Filly, A. R. Margulis, K. L. Moon, L. E. Crooks, L. Kaufman, *Radiology* **147**, 481 (1983); T_1 and T_2 change significantly with bile concentration (H. Hricak, personal communication).
64. H. Hricak, R. D. Williams, D. B. Spring, K. L. Moon, *Am. J. Roentgenol.* **141**, 1101 (1983).
65. H. K. Genant, K. L. Moon, N. I. Chafetz, C. A. Helms, in *Clinical Magnetic Resonance Imaging*, A. R. Margulis *et al.*, Eds. (Radiology Research and Education Foundation, San Francisco, 1983), pp. 251–276; M. T. Modic *et al.*, *Am. J. Roentgenol.* **141**, 1129 (1983).
66. M. T. Modic *et al.*, *Radiology* **152**, 103 (1984).
66a. See B. D. Ross *et al.*, in (*4*); see also R. H. T. Edwards *et al.*, in *ibid.*
67. T. F. Budinger and C. Cullander, in *Biomedical Magnetic Resonance*, T. L. James and A. R. Margulis, Eds. (Radiology Research and Education Foundation, San Francisco, 1984), pp. 421–441.
68. Revised guidance on acceptable limits of exposure during NMR clinical imaging is given in *Br. J. Radiol.* **56**, 974 (1983). The U.S. Food and Drug Administration guidelines specify 0.4 W/kg but not a specific temperature elevation criterion.
69. Visual phosphenes are perceived light flickers or flashes of brief duration induced by momentary pressure on the eyeball or by electric currents and changing magnetic fields in the vicinity of the human eye [T. F. Budinger, *IEEE Trans. Nucl. Sci.* **NS-26**, 2821 (1979); P. Lovsund, S. E. G. Nilsson, T. Reuter, P. Oberg, *Med. Biol. Eng. Comput.* **18**, 326 (1980)].
70. P. A. Oberg, *Med. Biol. Eng.* **11**, 55 (1973); S. Ueno, S. Matsumoto, K. Harada, Y. Oomura, *IEEE Trans. Magn.* **14**, 5 (1978); M. J. R. Poulson, A. T. Barker, A. T. Freeston, II, *Med. Biol. Eng. Comput.* **20**, 243 (1982).
71. P. F. J. New *et al.*, *Radiology* **147**, 139 (1983); P. L. Davis, L. Crooks, M. Arakawa, R. McRee, L. Kaufman, A. R. Margulis, *Am. J. Roentgenol.* **137**, 857 (1981); W. Pavlicek *et al.*, *Radiology* **147**, 149 (1983); R. L. Soulen, T. F. Budinger, C. B. Higgins, *ibid.*, in press.
72. Measurements were made by T. F. Budinger and C. Cullander on the Washington, D.C., Metro and on the San Francisco BART transit systems, using a Hall effect magnetometer calibrated at the Lawrence Berkeley Laboratory, University of California.
73. We thank S. Koenig, M. Roos, and G. Stimack for their contributions. Technical and clinical perspectives were critiqued by T. Brown, A. Margulis, W. Carrera, P. Valk, and G. Wolf. C. Green and A. Suttle motivated this work. Manuscript preparation was supported by IBM Instruments, the National Institutes of Health, and the Department of Energy.

Laser Chemical Analysis

Richard N. Zare

Summary. Selected applications of laser methods to analytical problems are reviewed. Examples are chosen from multiphoton ionization and laser fluorescence analysis. Although efforts to carry out elemental analysis with laser techniques are probably the most advanced, studies suggest that the analysis of molecular species is also quite promising, particularly in regard to interfacing laser fluorimetric detection with high-performance liquid chromatography. Recent experiments indicate that analysts can expect to attain in a number of cases the ultimate limit of single-atom or single-molecule detection with laser-based methods.

The intimate association of chemistry and light ranges from fireworks displays and the color of solutions and precipitates to the spectroscopic analysis of new and unknown substances. The advent of the laser has only served to strengthen this natural bond, so that no major chemical research laboratory is without lasers today. Because of its high power, directionality, purity of color, and temporal coherence, the laser has become a highly versatile tool, first applied to the study of how chemical reactions occur, then to initiate chemical reactions upon irradiation, and finally as an extremely sensitive and selective means to analyze for the presence of chemical substances of interest. It is this last topic which is the subject of this brief selective review in which outstanding examples of recent advances in chemical analysis based on laser techniques are presented. Laser methodologies promise to improve dramatically the detection of trace substances embedded in "real" matrices, giving the analyst a most powerful means for determining the composition of materials.

Richard N. Zare is Shell Distinguished Professor of Chemistry in the Department of Chemistry, Stanford University, Stanford, California 94305.

Multiphoton Ionization

One of the most promising laser techniques is multiphoton ionization (MPI), in which an atom or molecule absorbs more than one photon to cause ejection of an electron (*1*, *2*). This nonlinear process is made possible by the high intensity of laser light sources. We first review how the MPI process works, then describe some recent applications.

Figure 1 compares multiphoton ionization to single-photon ionization. If the energy of the photon exceeds the ionization energy of the target atom or molecule, the target species will be ionized and can be detected by measuring the subsequent positively charged ion or negatively charged photoelectron (Fig. 1a). If, however, the energy of one photon lies below the ionization threshold, ionization can occur only by the simultaneous absorption of several photons whose energy sum exceeds the ionization potential (Fig. 1, b and c). Multiphoton processes may involve virtual levels (Fig. 1b) which are not eigenstates (real levels) of the isolated atom or molecule. The lifetime for such virtual levels is often on the order of 10^{-15} second. The MPI process is said to be resonant when the energy of an integral number, n, of photons approaches closely the energy of an n-photon–allowed transition. Because real levels have lifetimes typically of 10^{-9} to 10^{-6} second, the probability for absorbing subsequent photons is greatly increased (six orders of magnitude or more). Consequently, nonresonant multiphoton ionization usually requires laser powers of about 1 GW/cm^2, which can be achieved only by tightly focusing powerful pulsed lasers. In contrast, resonant enhanced multiphoton ionization (REMPI), also called resonance ionization spectroscopy (RIS), can be carried out with pulsed lasers of fairly modest intensity (1 MW/cm^2) and under favorable conditions even with continuous-wave laser sources. The